Journal of Power Sources 217 (2012) 562–568

Contents lists available at SciVerse ScienceDirect

Journal of Power Sources

journal homepage: www.elsevier.com/locate/jpowsour

Direct peroxide–peroxide fuel cell – Part 1: The anode and cathode catalyst of carbon fiber cloth supported dendritic Pd

Fan Yang, Kui Cheng, Yinghua Mo, Liqiu Yu, Jingling Yin, Guiling Wang, Dianxue Cao*

Key Laboratory of Superlight Material and Surface Technology of Ministry of Education, College of Material Science and Chemical Engineering, Harbin Engineering University, Harbin 150001, China

HIGHLIGHTS

- Dendritic Pd is electrodeposited on CFC via potential pulse technique.
- Pd/CFC electrode shows high catalytic activity for H_2O_2 oxidation and reduction.
- Pd/CFC electrode shows a unique open structure to make the full utilization of Pd.

ARTICLE INFO

Article history:
Received 15 May 2012
Received in revised form
4 July 2012
Accepted 6 July 2012
Available online 17 July 2012

Keywords:
Dendritic palladium
Carbon fiber cloth
Hydrogen peroxide
Electrooxidation
Electroreduction
Fuel cell

ABSTRACT

Dendritic Pd is electrodeposited uniformly on carbon fiber cloth via a potential pulse technique. The electrode is characterized by scanning electron microscopy, transmission electron microscopy and X-ray diffractometer, and it shows a unique open structure allowing the full utilization of Pd surface active sites. H_2O_2 electrooxidation in KOH solution and electroreduction in H_2SO_4 solution on the dendritic Pd electrode are studied by linear sweep voltammetry and chronoamperometry. The electrode exhibits a high catalytic performance for both H_2O_2 electrooxidation and electroreduction, and it outperforms the conventional electrode made with commercial Pd/C powder. KOH and H_2SO_4 in excess show no improvement to the activity of H_2O_2 oxidation and reduction, respectively. The overpotential at the same current density for H_2O_2 electrooxidation in alkaline solution is significantly lower than that for electroreduction in acid medium on the dendritic Pd electrode.

1. Introduction

Hydrogen peroxide (H_2O_2) has been investigated as the oxidant (Eqs. (1) and (3)) of liquid-based fuel cells for use in air-free environments (space and underwater) due to its faster reduction kinetics and easier storage and handling than gaseous oxygen [1–9]. H_2O_2 can also be used as the fuel of fuel cells because it can be electrooxidized to oxygen (Eqs. (2) and (4)). Recent studies on the open circuit potentials (OCP) of H_2O_2 in acidic and basic electrolytes demonstrated that the OCP is a mixed potential of H_2O_2 electroreduction (Eqs. (1) and (3)) and electrooxidation (Eqs. (2) and (4)) simultaneously occurring at electrode surfaces and it is more close to the equilibrium potential of H_2O_2 electrooxidation (e.g. ~0.8 V in acid and ~0.1 V in alkaline at Pd electrode) [10]. Based on this result, there exists a potential difference between H_2O_2 reduction in acid and oxidation in base. This provides a theory basis for direct peroxide–peroxide fuel cell using H_2O_2 both as the fuel (in alkaline electrolyte) and the oxidant (in acid electrolyte).

$$H_2O_2 + 2H^+ + 2e^- \rightarrow 2H_2O \quad E^0 = 1.776\ V \tag{1}$$

$$H_2O_2 \rightarrow O_2 + 2H^+ + 2e^- \quad E^0 = -0.695\ V \tag{2}$$

$$HO_2^- + H_2O + 2e^- \rightarrow 3OH^- \quad E^0 = 0.878\ V \tag{3}$$

$$HO_2^- + OH^- \rightarrow O_2 + H_2O + 2e^- \quad E^0 = 0.146\ V \tag{4}$$

Yamazaki et al. [11] reported a H_2O_2 fuel cell using H_2O_2 both as the oxidant and the fuel. This cell has a one-compartment configuration using NaOH electrolyte without the membrane for the separation of anode and cathode. By carefully selecting the suitable

* Corresponding author. Tel./fax: +86 451 82589036.
E-mail address: caodianxue@hrbeu.edu.cn (D. Cao).

0378-7753/$ – see front matter © 2012 Elsevier B.V. All rights reserved.
http://dx.doi.org/10.1016/j.jpowsour.2012.07.019

anode and cathode catalysts, the fuel cell was able to generate a maximum current density of 2.9 mA cm^{-2} and achieved an open circuit voltage of around 100 mV. Obviously, the performance of such a H_2O_2 cells is quite low. Later on, Sanli and Aytaç [12] reported a two-compartment H_2O_2 fuel cell having the conventional fuel cell configuration. By separating the anode and cathode compartments and operating with basic H_2O_2 as fuel and acidic H_2O_2 as oxidant, the cell demonstrated an open circuit voltage of around 0.9 V and a peak power density of 3.8 mW cm^{-2}. So the performance of H_2O_2 fuel cell needs to significantly improve in order compete with other types of fuel cells.

Electrocatalyst plays key roles for improvements of the performance of a fuel cell. Some types of electrocatalysts for H_2O_2 oxidation and reduction have been investigated, which include noble metals [4,13–16], transition metal oxides [17,18] and macrocycle complexes of transition metals [2,19]. Noble metals show promising performance because they have high catalytic activity for both H_2O_2 electroreduction and electrooxidation and have good stability. In general, noble metals are loaded on carbon black to form powder catalysts. They are mixed with conducting carbons and polymer binders to form pastes, and then applied to a carbon paper current collector. Such obtained electrodes usually suffer drawbacks of low catalyst utilization because some catalysts are unable to contact with the current collector and electrolyte to form the three-phase reaction zone [20–22]. In addition, if gas products were involved (e.g. methanol oxidation, borohydride hydrolysis), they may block the active sites of catalysts causing a reduction of catalytic efficiency due to the slow removal of gas bubbles from compact electrodes.

In this work, we report a novel Pd electrode with open structure. Dendritic Pd particles were deposited onto carbon fiber cloth (CFC) by potential pulse electrodeposition. Pd was selected as the catalyst because it is a non-platinum catalyst with good stability in the harsh acidic and basic H_2O_2 solution. CFC with open channels was used both as the support and the current collector to enable the electrode to have good mass transport property. The obtained electrode (Pd/CFC) demonstrated high activity and good stability for H_2O_2 electrooxidation in KOH solution (the anode reaction of the H_2O_2 fuel cell) and electroreduction in H_2SO_4 solution (the cathode reaction of the H_2O_2 fuel cell). In part 2 of this series [23], we showed that a H_2O_2 fuel cell with the Pd/CFC anode and cathode displayed a much higher performance than that reported in literatures.

2. Experimental

2.1. Reagents

Palladium(II) chloride (>99.9%), sulfuric acid, potassium hydroxide, perchloric acid and hydrogen peroxide were obtained from Enterprise Group Chemicals Reagent Co. Ltd. China. Carbon fiber cloth (thickness: 0.3 mm) and commercial Pd/C (20 wt %) were purchased from Shanghai Hesen electric Co., Ltd. All chemicals are analytical grade and were used as-received without further purification. Ultrapure water (Millipore, 18 MΩ cm) was used throughout the study.

2.2. Preparation and characterization of the Pd/CFC electrode

The Pd/CFC electrodes were prepared by potential pulse electrodeposition (Scheme 1) of Pd onto CFC using 5.0 mmol dm^{-3} $PdCl_2$ + 0.1 mol dm^{-3} $HClO_4$ as the deposition solution. The depositions were carried out in a three-electrode electrochemical cell controlled by computerized potentiostat (Autolab PGSTAT302, Eco Chemie). The CFC (1.0 × 1.0 cm) served as the working

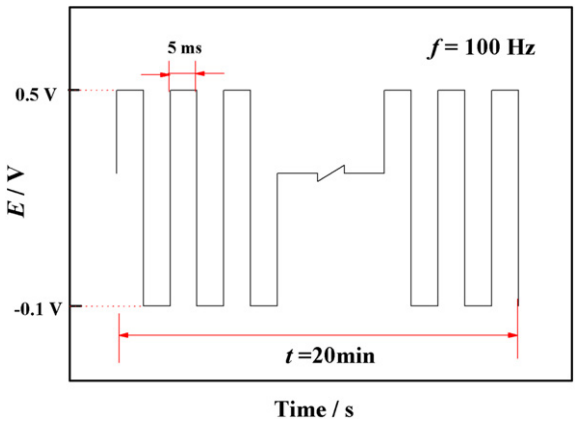

Scheme 1. The potential waves for the deposition of dendritic Pd on CFC.

electrode, which was placed between two pieces of platinum foil (1.0 × 1.0 cm) in parallel as the counter electrodes. A saturated Ag/AgCl (3 mol dm^{-3} KCl) electrode was used as the reference electrode, and all potentials in this work were referred to this reference electrode.

The oxidation and reduction potential, the deposition time and the concentration of $PdCl_2$ were found to have a significant effect on the morphology of Pd deposited on the CFC substrate. In order to check the influence of oxidation potential (upper potential), the reduction potential (lower potential) was kept at −0.15 V, the deposition time was set to be 20 min and the solution concentration was maintained in 5.0 mmol dm^{-3} $PdCl_2$ + 0.1 mol dm^{-3} $HClO_4$, the upper potential was varied (0.85 V, 0.65 V, 0.60 V, 0.55 V, 0.50 V). It was found that, at high oxidization potential (e.g. 0.85 V), Pd nanoparticles were formed on the CFC, instead of the dendritic Pd. When the oxidization potential was reduced, Pd nanorods were first observed, and then the dendritic-like Pd was formed at 0.50 V. The effect of the reduction potential was also investigated in the range of 0.10 ~ −0.15 V by fixing the oxidization potential at 0.50 V. It was found that the Pd morphology changed dramatically with the change of reduction potential. With the decrease of the reduction potential, Pd was transferred from nanoparticle aggregates to flower-like nanostructures and then to dendrites. The deposition time and the concentration of $PdCl_2$ solution show similar effects on the Pd morphology, that is, shortening the reduction time or reducing the solution concentration decreased the length of Pd dendrites. Studies on the catalytic performance of the Pd/CFC electrodes with different morphology of Pd (nanoparticle, nanorod, flower-like structure, and dendrite) for H_2O_2 electrooxidation and electroreduction demonstrated that the dendritic Pd/CFC electrode displayed the highest performance among the four types of electrodes. The dendritic Pd/CFC electrode used in this study was prepared under the following condition (Scheme 1): The oxidation potential is 0.50 V, the reduction potential is −0.10 V, the frequency of the potential pulse is 100 Hz, the deposition time is 20 min, and the deposition solution is 5.0 mmol dm^{-3} $PdCl_2$ + 0.1 mol dm^{-3} $HClO_4$.

The electrode morphology was characterized by a scanning electron microscope (SEM, JEOL JSM-6480) and a transmission electron microscope (TEM, FEI Teccai G2S-Twin, Philips). The structure was analyzed using an X-ray diffractometer (Rigaku TTR III) with Cu Kα radiation (λ = 0.1514178 nm). The Pd loading was measured using an inductive coupled plasma emission spectrometer (ICP, Xseries II, Thermo Scientific). Pd in the 1.0 cm^2 electrode was first dissolved in aqua regia solution and then diluted to 1000 dm^3 solution for the ICP measurement.

2.3. Electrochemical measurements

H_2O_2 electrooxidation and electroreduction were performed in a three-electrode electrochemical cell with the same configuration as that for electrodeposition with the exception that the two Pt foil counter electrodes were placed behind D-porosity glass frits. The electrolyte for H_2O_2 electrooxidation and electroreduction was H_2O_2-containing KOH and H_2SO_4 solution, respectively. The reported current densities were calculated using the geometrical area of the electrode. All solutions were made with analytical grade chemical reagents and ultra-pure water (Milli-Q 18 MΩ cm). All measurements were performed at ambient temperature (20 ± 2 °C) under N_2 atmosphere.

3. Results and discussion

3.1. Characterization of the Pd/CFC electrode

Fig. 1 shows the XRD patterns of the CFC substrate and the Pd/CFC electrode. The CFC displayed three broad peaks centered at about 23°, 43° and 80°, which can be associated with carbon. The sharp diffraction peaks at 40°, 46°, 68°, 82° observed on the Pd/CFC electrode matched well with the (1 1 1), (2 0 0), (2 2 0), and (3 1 1) plane of Pd, respectively, according to the standard crystallographic spectrum of Pd (JCPDS card No. 65-2867). These peaks indicated that Pd has a face-centered cubic (fcc) structure and presents as the metallic state.

Fig. 2 shows the SEM images of the CFC substrate and the Pd/CFC electrode. The CFC is composed of cross-oriented carbon fiber bundles weaving together. There exist void spaces between carbon fibers, which allow electrolytes to access the full electrode surface. Besides, the high electrical conductivity and the flexibility of CFC make it an ideal candidate for the support of Pd catalysts. As seen from Fig. 2b–d, Pd was uniformly deposited onto carbon fiber surface and it shows a dendrite-like microstructure. The spindly leaves of the Pd dendrite have lengths up to around 2 μm, middle diameters up to around 500 nm and tip diameters down to around a few nanometers. This feature is further confirmed by the TEM image of a single leave (insert of Fig. 2d). The unique structure of the Pd/CFC electrode ensured the full utilization of Pd surfaces because all the Pd particles are accessible to H_2O_2 and electrolytes. Besides, oxygen gas generated by H_2O_2 electrooxidation or hydrolysis can quickly diffuse away from the electrode, preventing surface active sites of Pd from blocking by adsorbed gas bubbles.

Fig. 3a and b show the cycle voltammograms (CV) of the CFC and the Pd/CFC electrode measured in 1.0 mol dm^{-3} H_2SO_4 and 1.0 mol dm^{-3} KOH solution at a scan rate of 50 mV s^{-1}, respectively.

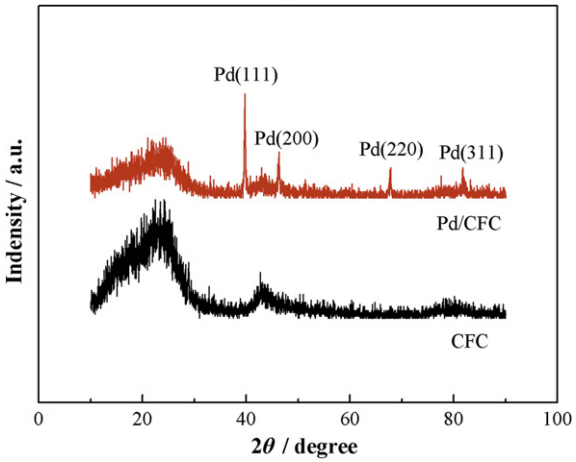

Fig. 1. XRD pattern of CFC and Pd/CFC.

The CV of the CFC substrate only showed double layer current in both KOH and H_2SO_4 solution. The CV of the Pd/CFC electrode displayed the typical features of polycrystalline Pd, which are similar to those reported in the literature for a Pd electrode in alkaline and acid solution [9,24–26]. The hydrogen adsorption/desorption and surface oxide formation/reduction peaks are clearly seen and well defined. So the CV demonstrated that Pd was electrodeposited on the CFC substrate as polycrystalline metal. The charge obtained from the cathodic peak centered at 0.43 V in Fig. 3a was employed to estimate the electrochemically active surface area of Pd assuming that a monolayer of PdO was formed and its reduction charge value is 405 μC cm^{-2} [27,28]. Such estimated electrochemically active surface area (EASA) is 68.2 cm^2. ICP measurement shows that the Pd loading is 0.3061 mg. So the specific EASA of Pd reached 22.3 m^2 g^{-1}, which is close to that of Pd nanoparticles supported on carbon materials reported in literatures [29,30]. For example, Yang et al. [30] reported that the multi-walled carbon nanotubes supported Pd nanoparticles have a specific EASA of 21.4 m^2 g^{-1}. High specific EASA usually means high utilization of Pd, which is important for the reduction of the cost of precious metal catalysts.

3.2. H_2O_2 electrochemical oxidation and reduction on the Pd/CFC electrode

Since H_2O_2 electrooxidation in alkaline electrolyte occurs at lower potential than its electroreduction in acid electrolyte, H_2O_2 can be used as both the fuel (with alkaline anolyte) and the oxidant (with acidic catholyte), and thus a direct H_2O_2–H_2O_2 fuel cell can be built. Prior to demonstrate such a fuel cell, we first investigated H_2O_2 electrooxidation in alkaline KOH solution and its electroreduction in acidic H_2SO_4 solution on the Pd/CFC electrode. According to Eqs. (1) and (4), besides acting as electrolytes, KOH and H_2SO_4 also take part in the oxidation and reduction of H_2O_2, respectively. So we systemically studied the effect of the concentration of H_2O_2, KOH and H_2SO_4 on the catalytic performance of Pd/CFC electrode in order to better understand the anode and the cathode behavior of direct H_2O_2–H_2O_2 fuel cell.

3.2.1. H_2O_2 electroreduction in H_2SO_4 solution at the Pd/CFC electrode

Fig. 4 shows the effect of H_2SO_4 concentration on the electroreduction of H_2O_2 at Pd/CFC electrode. The concentration of H_2O_2 was fixed at 0.5 mol dm^{-3} and the concentration of H_2SO_4 varied from 1.0 to 3.0 mol dm^{-3} in order to maintain the ratio of $[H^+]/[H_2O_2]$ to be higher than 2 (Eq. (1)) considering H_2SO_4 is also the supporting electrolyte. As can be seen that excess amount of H_2SO_4 did not improve the activity of H_2O_2 electroreduction at Pd/CFC electrode. In contrast, too high concentration of H_2SO_4 (e.g. 3.0 mol dm^{-3} corresponding to $[H^+]/[H_2O_2]$ of 12) led to a slight decrease in the activity of H_2O_2 reduction. The maximum current density reached 175 mA cm^{-2} in 1.0 mol dm^{-3} H_2SO_4 + 0.5 mol dm^{-3} H_2O_2 ($[H^+]/[H_2O_2] = 2$). Two reduction peaks can be seen, particularly at high concentration of H_2SO_4, which may suggest different reaction steps. The following mechanism for H_2O_2 electroreduction in acidic media has been proposed (Eqs. (5) and (6)) [31,32]:

$$H_2O_2 + H^+ + e^- \xrightarrow{\text{slow}} OH_{(ads)} + H_2O \quad (5)$$

$$H^+ + OH_{(ads)} + e^- \xrightarrow{\text{fast}} H_2O \quad (6)$$

the first reduction peak occurring at around 0.5 V might be attributed to Eq. (5) and the second peak appeared at around 0.1 V

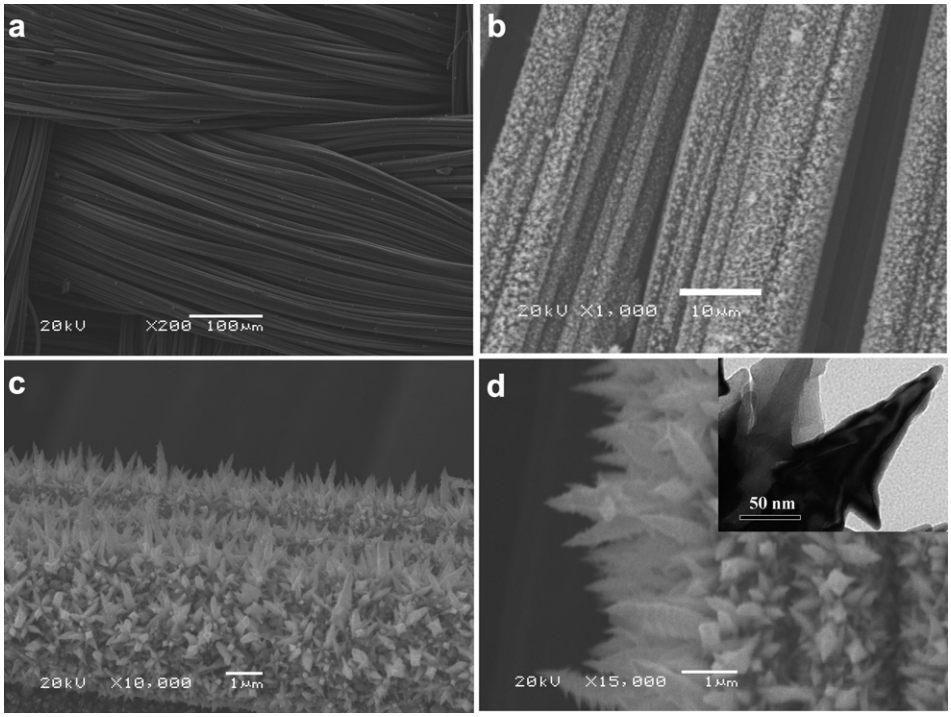

Fig. 2. SEM images of CFC (a) and Pd/CFC (b, c and d) and TEM image of Pd (inset of d).

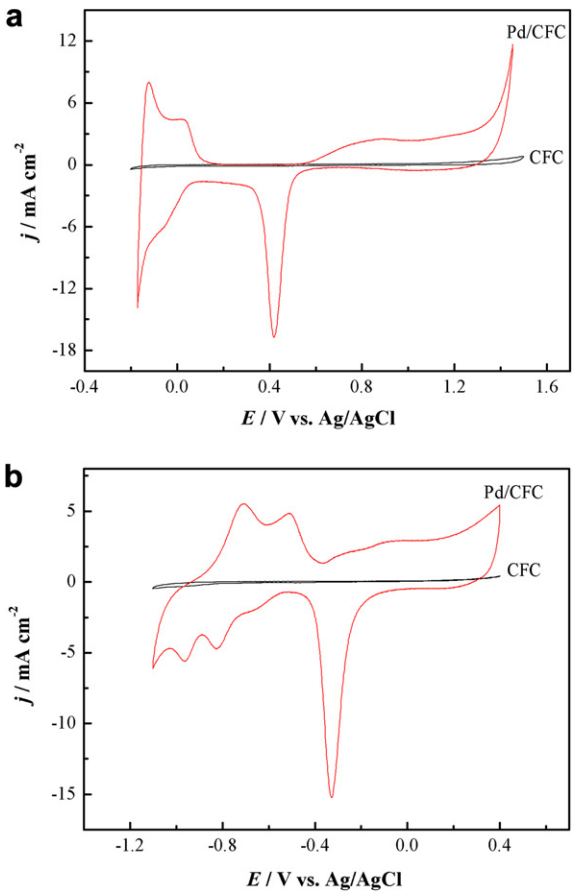

Fig. 3. Cyclic voltammograms of CFC and Pd/CFC electrode in 1.0 mol dm^{-3} H_2SO_4 (a) and 1.0 mol dm^{-3} KOH (b) at a scan rate of 50 mV s^{-1}.

to Eq. (6). The Eq. (5) provides the initial source of $OH_{(ads)}$, which, in turn, allows the reaction Eq. (6) to proceed at a faster rate.

Fig. 5 shows the effect of H_2O_2 concentration on the catalytic behavior of Pd/CFC electrode. The onset reduction potential was about 0.56 V and is nearly independent of the concentration of H_2O_2, which is in good agreement with the literature results [10]. The current density at the same potential increased significantly with the increase of H_2O_2 concentration from 0.5 to 2.0 mol dm^{-3}, but the further increase of H_2O_2 concentration from 2.0 to 2.5 mol dm^{-3} only leads to a slight increase of current density. Notably, the ratio of $[H^+]/[H_2O_2]$ at 2.0 mol dm^{-3} H_2O_2 is 2, which is the stoichiometric coefficient of H_2O_2 electroreduction in acid electrolyte (Eq. (1)). We noticed that chemical decomposition of H_2O_2 (indicated by the formation of gas bubbles on the electrode surface) became significant at H_2O_2 concentration higher than 2.0 mol dm^{-3}. Therefore, based on the results obtained from Figs. 4

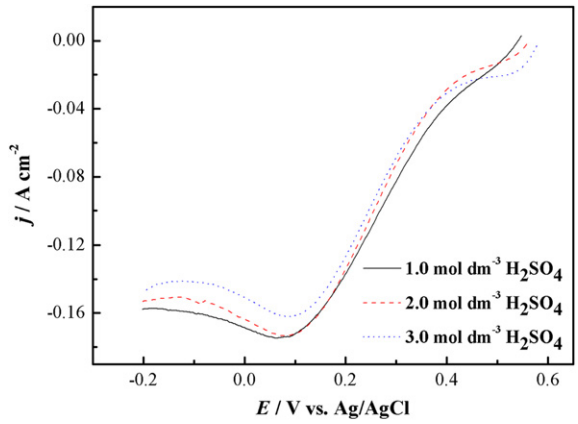

Fig. 4. Polarization curves for the Pd/CFC electrode in x mol dm^{-3} H_2SO_4 + 0.5 mol dm^{-3} H_2O_2 (x = 1.0, 2.0 and 3.0. Scan rate: 10 mV s^{-1}).

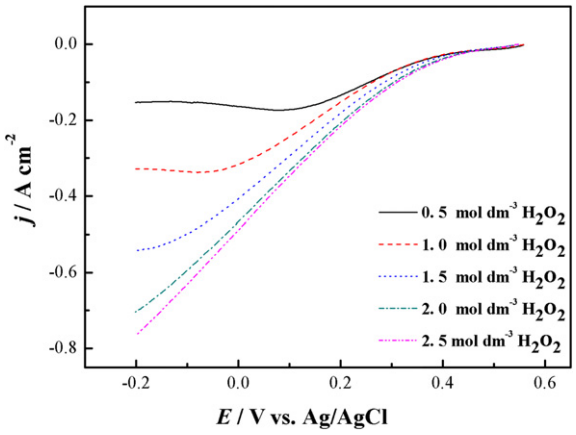

Fig. 5. Polarization curves for the Pd/CFC electrode in 2.0 mol dm^{-3} H_2SO_4 + x mol dm^{-3} H_2O_2 (x = 0.5, 1.0, 1.5, 2.0, and 2.5. Scan rate: 10 mV s^{-1}).

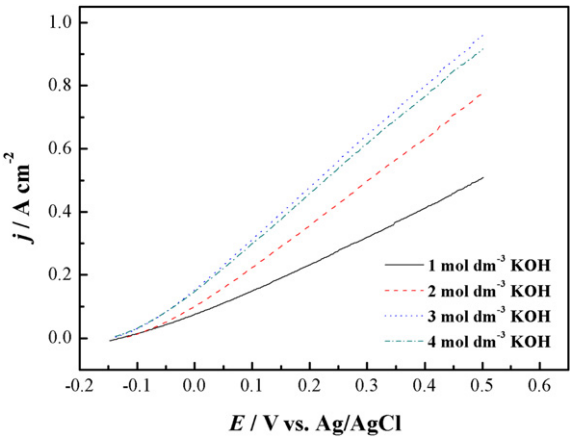

Fig. 7. Polarization curves for the Pd/CFC electrode in x mol dm^{-3} KOH + 0.5 mol dm^{-3} H_2O_2 (x = 1.0, 2.0, 3.0 and 4.0. Scan rate: 10 mV s^{-1}).

and 5, it can be concluded that the suitable ratio of $[H^+]/[H_2O_2]$ should be around 2.

Fig. 6 shows chronoamperometric curves for H_2O_2 reduction measured in 2.0 mol dm^{-3} H_2SO_4 containing 1.0 mol dm^{-3} H_2O_2. At 0.45 V (kinetic control region), current densities reached steady-state after a few seconds and displayed no decrease within 30 min test period. At 0.25 and 0.15 V (mixed kinetic-diffusion control region), current densities slightly decreased, which may result from the depletion of H_2O_2 near the electrode surface. The current density after 30 min reaction at 0.45, 0.25 and 0.15 V was 13, 67 and 120 mA cm^{-2}, respectively. Overall, the Pd/CFC electrode exhibits a good stability for hydrogen peroxide reduction. No obvious chemical decomposition of H_2O_2 was observed during the tests.

3.2.2. H_2O_2 electrooxidation in KOH solution at the Pd/CFC electrode

Fig. 7 shows the influence of KOH concentration on the electrooxidation of H_2O_2 at the Pd/CFC electrode. The concentration of H_2O_2 was kept at 0.5 mol dm^{-3}. The onset potential for H_2O_2 electrooxidation at Pd/CFC is about −0.15 V, independent of the concentration of KOH. While the current density at a same oxidation potential increased with the increase of KOH concentration up to 3.0 mol dm^{-3}, and remained nearly unchanged with the further increase of KOH concentration to 4.0 mol dm^{-3}. Similar to the electroreduction in H_2SO_4, excess electrolyte made no contribution to the enhancement of the activity of H_2O_2 oxidation. Interestingly, the polarization curves of current density against potential are approximately straight lines without any peaks. This is likely because that H_2O_2 electrooxidation generates O_2 gas (Eq. (4)) and the release of gas bubbles from the Pd/CFC electrode surface agitates the solution, thus makes the concentration of the reactants at the electrode surface and in the bulk solution is nearly the same. So the diffusion layer cannot be formed.

Fig. 8 demonstrates the dependence of the catalytic activity of the Pd/CFC on H_2O_2 concentration. The onset potential for H_2O_2 electrooxidation clearly shifted to negative value by around 50 mV when the concentration of H_2O_2 increased from 0.5 to 1.0 mol dm^{-3}, and is independent of the H_2O_2 concentration when it is higher than 1.0 mol dm^{-3}. The oxidation current density at low potential (below around 0.15 V) slightly increased with the increase of H_2O_2 concentrations up to 1.0 mol dm^{-3}. Basically, no significant change occurs when the concentration of H_2O_2 is higher than 1.0 mol dm^{-3}. It is worth to note that the H_2O_2 decomposition rate in KOH is faster at higher H_2O_2 concentration. So in order to maintain a high utilization of H_2O_2 fuel, its concentration in KOH solution should be kept as low as possible.

Fig. 9 shows the chronoamperometric curves for H_2O_2 electrooxidation in 3.0 mol dm^{-3} KOH and 1.0 mol dm^{-3} H_2O_2. It can be seen that larger current density was obtained at higher oxidation potential. The oxidation currents at each potential remained nearly

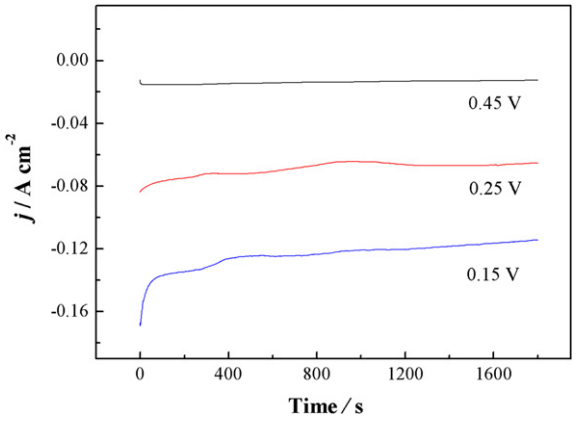

Fig. 6. Chronoamperometric curves for H_2O_2 electroreduction at different potentials in 2.0 mol dm^{-3} H_2SO_4 + 1.0 mol dm^{-3} H_2O_2.

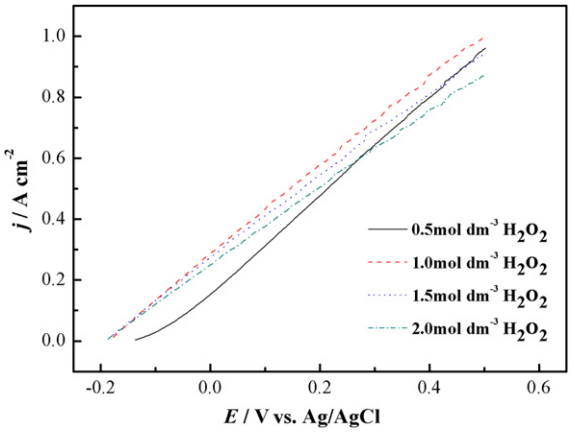

Fig. 8. Polarization curves for the Pd/CFC electrode in 3.0 mol dm^{-3} KOH + x mol dm^{-3} H_2O_2 (x = 0.5, 1.0, 1.5, and 2.0. Scan rate: 10 mV s^{-1}).

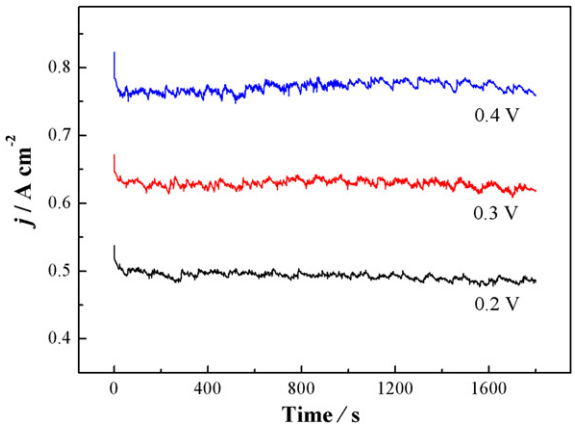

Fig. 9. Chronoamperometric curves for H_2O_2 electrooxidation at different potentials in 3.0 mol dm^{-3} KOH + 1.0 mol dm^{-3} H_2O_2.

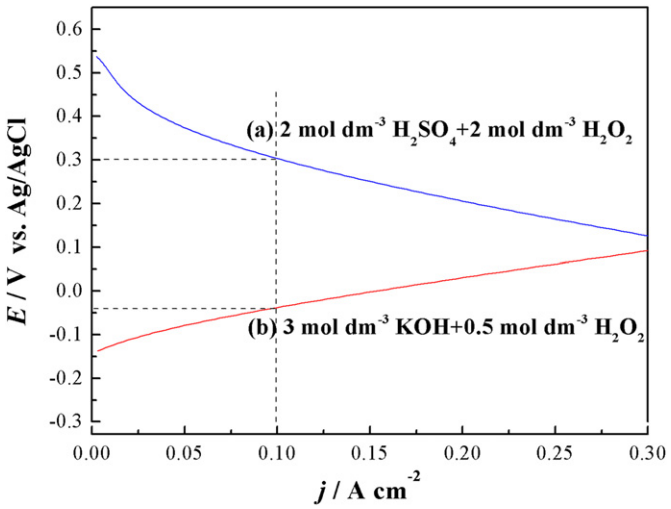

Fig. 10. Polarization curves for H_2O_2 electroreduction in H_2SO_4 (a) and electrooxidation in KOH (b) (Scan rate: 10 mV s^{-1}).

constant within the test period. It should be pointed out that all the chronoamperometric curves for H_2O_2 electroreduction (Fig. 6) and electrooxidation (Fig. 9) were tested using the same Pd/CFC electrode, which means the electrode was tested at different constant potentials for 3 h in total and still showed no decrease in catalytic performance. It is also worth to mention that the electrooxidation and electroreduction of H_2O_2 are quite simple reactions and the products are only O_2 and H_2O. So there is less possibility that the catalyst is poisoned. Differing from the smooth current–time curves for H_2O_2 electroreduction in H_2SO_4 (Fig. 6), the curves for H_2O_2 electrooxidation in KOH are quite rough with obvious current fluctuations. This phenomenon is caused by the formation and desorption of O_2 gas bubbles, which have been observed during the test. The current density after 30 min test at 0.2, 0.3 and 0.4 V was 493, 637 and 780 mA cm^{-2} respectively.

In a single direct H_2O_2–H_2O_2 fuel cell, the H_2O_2 electrooxidation and electroreduction occur concomitantly at the anode and the cathode, respectively, and therefore, the currents produced at the cathode and the anode are equal. Accordingly, through comparing the overpotentials of the anode and the cathode reaction at a same current density, which electrode limited the cell performance can be evaluated. The polarization curve for H_2O_2 electroreduction in H_2SO_4 (2.0 mol dm^{-3} H_2O_2 + 2.0 mol dm^{-3} H_2SO_4) and that for H_2O_2 electrooxidation in KOH (0.5 mol dm^{-3} H_2O_2 + 3.0 mol dm^{-3} KOH) were plotted in one figure (Fig. 10). The data were taken from Fig. 5 for the cathode reaction and Fig. 7 for the anode reaction. It can be seen that at the same current density, e.g. 100 mA cm^{-2}, the polarization overpotential for the cathode and the anode is around 300 mV and 38 mV, respectively. Clearly, the cathode has a much larger overpotential than the anode even though the cathode has a much higher concentration of H_2O_2. This implies that, for a direct H_2O_2–H_2O_2 fuel cell, the H_2O_2 concentration at the anode can be significant lower than that at the cathode. This is beneficial to the reduction of H_2O_2 decomposition in KOH anolyte solution. High concentration of H_2O_2 can be used at the cathode because H_2O_2 is more stable in acid than in alkaline solution.

In order to compare the catalytic performance of the dendritic Pd/CFC electrode with the electrode made with conventional carbon-supported Pd, commercial Pd/C (the Pd loading is 20 wt % and the carbon support is Vulcan XC72R) was applied to CFC to obtain an electrode with the Pd loading same as the dendritic Pd/CFC electrode (0.3061 mg cm^{-2}). The catalytic performance of the electrode made with the commercial Pd/C was compared with that of the dendritic Pd/CFC electrode, and the results are shown in Fig. 11. For H_2O_2 electroreduction (Fig. 11a), at potentials above ~0.33 V, the commercial Pd/C electrode exhibited slightly larger reduction current density than the dendritic Pd/CFC electrode. However, at potentials below ~0.33 V, the H_2O_2 reduction current density on the dendritic Pd/CFC electrode became obviously higher than that on the commercial Pd/C electrode. Fig. 11b clearly

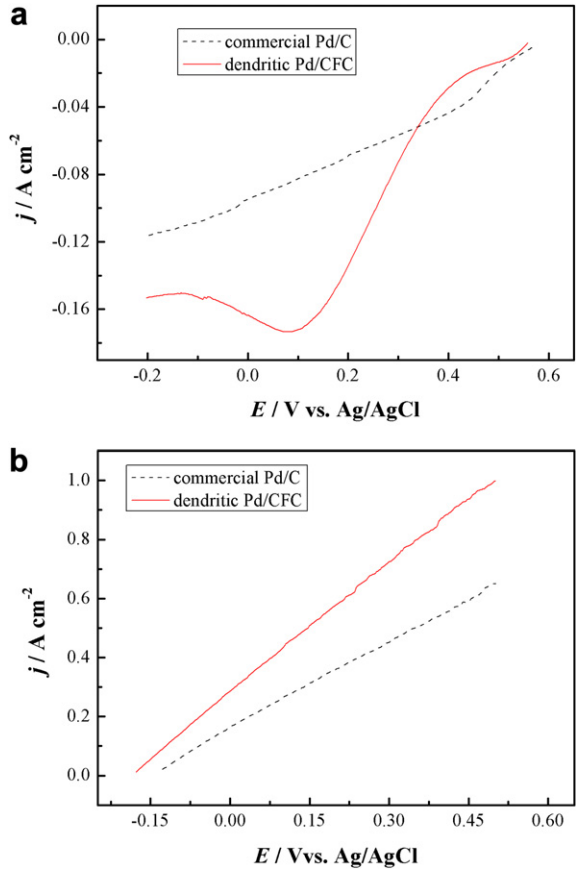

Fig. 11. Comparative polarization curves for (a) H_2O_2 electroreduction (solution: 1.0 mol dm^{-3} H_2SO_4 + 0.5 mol dm^{-3} H_2O_2. Scan rate: 10 mV s^{-1}) and (b) H_2O_2 electrooxidation (solution: 3.0 mol dm^{-3} H_2SO_4 + 1.0 mol dm^{-3} H_2O_2. Scan rate: 10 mV s^{-1}) at the dendritic Pd/CFC electrode and the electrode made with commercial Pd/C.

demonstrated that the dendritic Pd/CFC outperformed the commercial Pd/C electrode in the whole potential range for H_2O_2 electrooxidation. Similar results have been found in the studies of direct formic acid fuel cells (DFAFC) using the dendritic Pd/CFC as the anode. Shen et al. [33] reported that the peak power density of the DFAFC with a dendritic Pd/CFC anode was about 120 mW cm^{-2} and 240 mW mg^{-1} Pd. While, the peak power density using conventional Pd/C power electrode was only 50 mW cm^{-2}. So the DFAFC performance was remarkably enhanced by using the dendritic Pd/CFC anode to replace the conventional Pd/C power anode. Munichandraiah et al. [34] reported that the oxidation of formic acid on the dendritic Pd/C electrode takes place at −0.04 V, which is considerably lower (∼165 mV) than that on the nanoporous Pd/C electrode. So the dendritic Pd shows high catalytic performance than Pd/C power. Notably, conventional Pd/C electrodes are generally fabricated by mixing the dendritic Pd/C powder catalyst and polymer binders to form an ink, which is painted on Nafion@ membrane or carbon paper for the preparation of membrane electrolyte assembles (MEA). This MEA fabrication process is tedious and less controllable. The Pd/CFC was prepared by the simple electrochemical deposition of Pd directly onto CFC, which acted as the current collector. The obtained Pd/CFC electrode can be directly pressed onto Nafion@ to form the MEA.

4. Conclusions

Carbon fiber cloth supported dendritic Pd electrodes were successfully prepared through a potential pulse electrodeposition technique. Pd shows a corrugated dendritic structure and relatively uniformly distributed on the surface of carbon fibers. The unique open structure of the electrode enables the full utilization of Pd surfaces and allows the easy transportation of reactants to the catalyst as well as the quick removal of gaseous products from the electrode. The electrode demonstrated high catalytic activity and good stability for H_2O_2 electrooxidation in alkaline and electroreduction in acid solution and outperformed the conventional electrode made with commercial Pd/C powder. Under the same current density, the polarization overpotential for H_2O_2 electrooxidation in alkaline solution is significant lower than that for electroreduction in acid medium, which enable the use of low concentration of H_2O_2 at the anode, and thus ensure the high utilization of H_2O_2 fuel by reducing the chemical decomposition rate of H_2O_2 in the KOH anolyte.

Acknowledgments

We gratefully acknowledge the financial support of this research by National Nature Science Foundation of China (20973048), Fundamental Research Funds for the Central Universities (HEUCFT1205), Harbin Science and Technology Innovation Fund for Excellent Academic Leaders (2012RFXXG103), and Specialized Research Fund for the Doctoral Program of Higher Education (20102304110001).

References

[1] T. Bewer, T. Beckmann, H. Dohle, J. Mergel, D. Stolten, J. Power Sources 125 (2004) 1–9.
[2] D. Cao, J. Chao, L. Sun, G. Wang, J. Power Sources 179 (2008) 87–91.
[3] D. Cao, D. Chen, J. Lan, G. Wang, J. Power Sources 190 (2009) 346–350.
[4] D. Cao, Y. Gao, G. Wang, R. Miao, Y. Liu, Int. J. Hydrogen Energy 35 (2010) 807–813.
[5] S.J. Lao, H.Y. Qin, L.Q. Ye, B.H. Liu, Z.P. Li, J. Power Sources 195 (2010) 4135–4138.
[6] W. Sung, J.-W. Choi, J. Power Sources 172 (2007) 198–208.
[7] B. Tartakovsky, S.R. Guiot, Biotechnol. Prog. 22 (2006) 241–246.
[8] S.J. Lue, W.-T. Wang, K.P.O. Mahesh, C.-C. Yang, J. Power Sources 195 (2010) 7991–7999.
[9] D. Cao, L. Sun, G. Wang, Y. Lv, M. Zhang, J. Electroanal. Chem. 621 (2008) 31–37.
[10] X. Jing, D. Cao, Y. Liu, G. Wang, J. Yin, Q. Wen, Y. Gao, J. Electroanal. Chem. 658 (2011) 46–51.
[11] S.-i. Yamazaki, Z. Siroma, H. Senoh, T. Ioroi, N. Fujiwara, K. Yasuda, J. Power Sources 178 (2008) 20–25.
[12] A.E. Sanli, A. Aytaç, Int. J. Hydrogen Energy 36 (2011) 869–875.
[13] G.H. Miley, N. Luo, J. Mather, R. Burton, G. Hawkins, L. Gu, E. Byrd, R. Gimlin, P.J. Shrestha, G. Benavides, J. Laystrom, D. Carroll, J. Power Sources 165 (2007) 509–516.
[14] W. Yang, S. Yang, W. Sun, G. Sun, Q. Xin, J. Power Sources 160 (2006) 1420–1424.
[15] R.R. Bessette, M.G. Medeiros, C.J. Patrissi, C.M. Deschenes, C.N. LaFratta, J. Power Sources 96 (2001) 240–244.
[16] X. He, C. Hu, H. Liu, G. Du, Y. Xi, Y. Jiang, Sens. Actuators, B 144 (2010) 289–294.
[17] H. Liu, L. Zhang, J. Zhang, D. Ghosh, J. Jung, B.W. Downing, E. Whittemore, J. Power Sources 161 (2006) 743–752.
[18] V.L.N. Dias, E.N. Fernandes, L.M.S. da Silva, E.P. Marques, J. Zhang, A.L.B. Marques, J. Power Sources 142 (2005) 10–17.
[19] G. Wang, D. Cao, C. Yin, Y. Gao, J. Yin, L. Cheng, Chem. Mater. 21 (2009) 5112–5118.
[20] N. Cheng, H. Lv, W. Wang, S. Mu, M. Pan, F. Marken, J. Power Sources 195 (2010) 7246–7249.
[21] L. Feng, S. Yao, X. Zhao, L. Yan, C. Liu, W. Xing, J. Power Sources 197 (2012) 38–43.
[22] S. Ha, R. Larsen, R.I. Masel, J. Power Sources 144 (2005) 28–34.
[23] F. Yang, K. Cheng, X. Liu, S. Chang, J. Yin, C. Du, L. Du, G. Wang, D. Cao, J. Power Sources, in press.
[24] J.-P. Chevillot, J. Farcy, C. Hinnen, A. Rousseau, J. Electroanal. Chem. Interfacial Electrochem. 64 (1975) 39–62.
[25] T. Mallát, É. Polyánszky, J. Petró, J. Catal. 44 (1976) 345–351.
[26] E. Rikkinen, A. Santasalo-Aarnio, S. Airaksinen, M. Borghei, V. Viitanen, J. Sainio, E.I. Kauppinen, T. Kallio, A.O.I. Krause, J. Phys. Chem. C 115 (2011) 23067–23073.
[27] T. Chierchie, C. Mayer, W.J. Lorenz, J. Electroanal. Chem. Interfacial Electrochem. 135 (1982) 211–220.
[28] R. Pattabiraman, Appl. Catal., A 153 (1997) 9–20.
[29] R. Rego, C. Oliveira, A. Velázquez, P.-L. Cabot, Electrochem. Commun. 12 (2010) 745–748.
[30] C. Hu, Z. Bai, L. Yang, J. Lv, K. Wang, Y. Guo, Y. Cao, J. Zhou, Electrochim. Acta 55 (2010) 6036–6041.
[31] F.W. Campbell, S.R. Belding, R. Baron, L. Xiao, R.G. Compton, J. Phys. Chem. C 113 (2009) 9053–9062.
[32] G. Flätgen, S. Wasle, M. Lübke, C. Eickes, G. Radhakrishnan, K. Doblhofer, G. Ertl, Electrochim. Acta 44 (1999) 4499–4506.
[33] H. Meng, F. Xie, J. Chen, P.K. Shen, J. Mater. Chem. 21 (2011) 11352–11358.
[34] S. Patra, B. Viswanath, K. Barai, N. Ravishankar, N. Munichandraiah, ACS Appl. Mater. Interfaces 2 (2010) 2965–2969.